



Article

A Comparative Study on Cure Kinetics of Layered Double Hydroxide (LDH)/Epoxy Nanocomposites

Zohre Karami ¹, Seyed Mohammad Reza Paran ¹, Poornima Vijayan P. ^{2,*} ,
Mohammad Reza Ganjali ^{1,3}, Maryam Jouyandeh ¹ , Amin Esmaeili ⁴ , Sajjad Habibzadeh ⁵,
Florian J. Stadler ⁶ and Mohammad Reza Saeb ^{1,*}

¹ Center of Excellence in Electrochemistry, School of Chemistry, College of Science, University of Tehran, Tehran 11155-4563, Iran; zohrekarami.2013@yahoo.com (Z.K.); smrparan@gmail.com (S.M.R.P.); ganjali@ut.ac.ir (M.R.G.); Maryam.jouyande@gmail.com (M.J.)

² Department of Chemistry, Sree Narayana College for Women (affiliated to University of Kerala), Kollam, Kerala 691001, India

³ Biosensor Research Center, Endocrinology and Metabolism Molecular-Cellular Sciences Institute, Tehran University of Medical Sciences, Tehran 14535, Iran

⁴ Department of Chemical Engineering, School of Engineering Technology and Industrial Trades, College of the North Atlantic—Qatar, Arab League St, Doha 24449, Qatar; amin.esmaeili-khalil-saraei@polymtl.ca

⁵ Department of Chemical Engineering, Amirkabir University of Technology (Tehran Polytechnic), Tehran 1591639675, Iran; sajjad.habibzadeh@aut.ac.ir

⁶ College of Materials Science and Engineering, Shenzhen Key Laboratory of Polymer Science and Technology, Guangdong Research Center for Interfacial Engineering of Functional Materials, Nanshan District Key Lab for Biopolymers and Safety Evaluation, Shenzhen University, Shenzhen 518055, China; fjstadler@szu.edu.cn

* Correspondence: poornimavijayan2007@gmail.com (P.V.P.); mrsaeb2008@gmail.com (M.R.S.); Tel.: +91-940-0769509 (P.V.P.); +98-(912)-8264307 (M.R.S.)

Received: 23 June 2020; Accepted: 5 August 2020; Published: 9 August 2020



Abstract: Layered double hydroxide (LDH) minerals are promising candidates for developing polymer nanocomposites and the exchange of intercalating anions and metal ions in the LDH structure considerably affects their ultimate properties. Despite the fact that the synthesis of various kinds of LDHs has been the subject of numerous studies, the cure kinetics of LDH-based thermoset polymer composites has rarely been investigated. Herein, binary and ternary structures, including $[\text{Mg}_{0.75} \text{Al}_{0.25} (\text{OH})_2]^{0.25+} [(\text{CO}_3^{2-})_{0.25/2} \cdot \text{m} \text{H}_2\text{O}]^{0.25-}$, $[\text{Mg}_{0.75} \text{Al}_{0.25} (\text{OH})_2]^{0.25+} [(\text{NO}_3^-)_{0.25} \cdot \text{m} \text{H}_2\text{O}]^{0.25-}$ and $[\text{Mg}_{0.64} \text{Zn}_{0.11} \text{Al}_{0.25} (\text{OH})_2]^{0.25+} [(\text{CO}_3^{2-})_{0.25/2} \cdot \text{m} \text{H}_2\text{O}]^{0.25-}$, have been incorporated into epoxy to study the cure kinetics of the resulting nanocomposites by differential scanning calorimetry (DSC). Both integral and differential isoconversional methods serve to study the non-isothermal curing reactions of epoxy nanocomposites. The effects of carbonate and nitrate ions as intercalating agents on the cure kinetics are also discussed. The activation energy of cure (E_a) was calculated based on the *Friedman* and Kissinger–Akahira–Sunose (*KAS*) methods for epoxy/LDH nanocomposites. The order of autocatalytic reaction (m) for the epoxy/Mg–Al–NO₃ (0.30 and 0.254 calculated by the *Friedman* and *KAS* methods, respectively) was smaller than that of the neat epoxy, which suggested a shift of the curing mechanism from an autocatalytic to noncatalytic reaction. Moreover, a higher frequency factor for the aforementioned nanocomposite suggests that the incorporation of Mg–Al–NO₃ in the epoxy composite improved the curability of the epoxy. The results elucidate that the intercalating anions and the metal constituent of LDH significantly govern the cure kinetics of epoxy by the participation of nitrate anions in the epoxide ring-opening reaction.

Keywords: cure kinetics; epoxy; layered double hydroxide; Mg–Al; isoconversional model

1. Introduction

Clay nanomaterials are the most well-known family of minerals in the field of nanoscience and nanotechnology [1]. Layered double hydroxides (LDHs), also known as anionic clays, have a two-dimensional (2D) crystalline nanostructure with weak interlayer bonding forces in between the layers [2,3]. The general chemical formula of an LDH is $[M_{1-x}^{2+}M_x^{3+}(\text{OH})_2]_{x+} [A^{n-}]_{x/n} \cdot m\text{H}_2\text{O}$ made up of di- and trivalent metal cations (M^{2+} and M^{3+}) in octahedral units together with a variety of anionic groups (A^{n-}) that can locate in the gallery to neutralize the positive charge of the overall structure [4,5]. Acceptable physical and chemical properties of an LDH are accompanied by its facile synthesis with tunable chemical composition for various fields [6]. Moreover, the anion exchange properties of an LDH make possible its intercalation/exfoliation in the polymer matrix [7].

Many research works have been focused on the role of LDHs in the improvement of the properties of polymers, like anti-corrosion behavior, flame retardancy and mechanical properties [7–9]. It is well known that the ultimate properties of thermoset resins are dependent on network formation during cure reactions [10–12]. Overall, the incorporation of nanoparticles into the thermosetting polymers, e.g., epoxy, can tackle brittleness and low modulus drawbacks [13–16]. The study of curing allows for understanding the structure–properties relationship in thermoset nanocomposites [17–19]. However, network formation in epoxy resin is a complicated phenomenon because of gelation and vitrification, by gradual transformation from a chemical- to diffusion-controlled reaction in the system [20,21]. The *Cure Index (CI)* was recently defined as a simple criterion to elucidate the curability of thermoset composites [22,23]. It is a dimensional criterion for evaluating the quality of the curing process in thermoset systems. By the use of the *CI*, the curing potential of thermoset composites can be classified as *Poor*, *Good* or *Excellent* [24]. However, the quantitative analysis of cure reactions by analytical methods may shed more light on the role of nanoparticles [25–27].

The curability of epoxy nanocomposites with nanoparticles of various shapes, sizes and surface chemistry is comprehensively discussed by cure behavior and cure kinetics analyses [28,29]. In previous studies, we synthesized binary Mg–Al LDHs intercalated with carbonate and nitrate ions, as well as ternary Mg–Zn–Al LDHs intercalated with carbonate anions [30–32]. The use of the *CI* provided a rough image of the curability of the resulting nanocomposites, such that the enlargement of the gallery space of the LDH structure by anions supported network formation in the epoxy/LDH system. In the current study, the effects of the Mg–Al–CO₃, Mg–Al–NO₃ and Mg–Zn–Al–CO₃ LDH structure on curing kinetics of epoxy/amine systems were compared in terms of non-isothermal differential scanning calorimetry (DSC). Analyses were done using differential *Friedman* and integral Kissinger–Akahira–Sunose (*KAS*) isoconversional methods.

2. Materials and Methods

The cure potential of the neat epoxy and its nanocomposites, containing binary Mg–Al–CO₃, Mg–Al–NO₃ and ternary Mg–Zn–Al–CO₃ LDHs, was studied by non-isothermal DSC. The material specifications used in the synthesis of LDHs and epoxy nanocomposite preparation are introduced in Appendix A.1 of Appendix A. The preparation and characterization of epoxy nanocomposites, including Mg–Al–CO₃, Mg–Al–NO₃ and Mg–Zn–Al–CO₃ LDHs, are also explained in Appendices A.2 and A.3 of Appendix A, respectively. In brief, LDHs in 0.1 wt.% were used in nanocomposite preparation, and non-isothermal DSC was carried out at a heating rate (β) of 2, 5, 7 and 10 °C·min^{−1} to evaluate the cure reaction. Quantitative cure was carried out in terms of cure behavior and cure kinetics analyses based on the protocol of cure proposed for thermoset composites [23].

3. Results and Discussion

3.1. Cure Behavior Analysis

DSC thermograms for the neat epoxy and nanocomposites containing 0.1 wt.% of Mg–Al–CO₃, Mg–Al–NO₃ and Mg–Zn–Al–CO₃ LDHs at four heating rates of 2, 5, 7 and 10 °C·min^{−1} are shown in

Figure 1. The cure state (*Poor*, *Good* or *Excellent*) was reported in previous works [30–32]. The unimodal peak unconditionally observed in the DSC curves proved the assumption of single-step reaction kinetics. Moreover, the higher values of the heat of cure and peak temperature upon increasing the heating rate from 2 to 10 °C·min⁻¹ are due to the higher kinetic energy per molecule in the system [17].

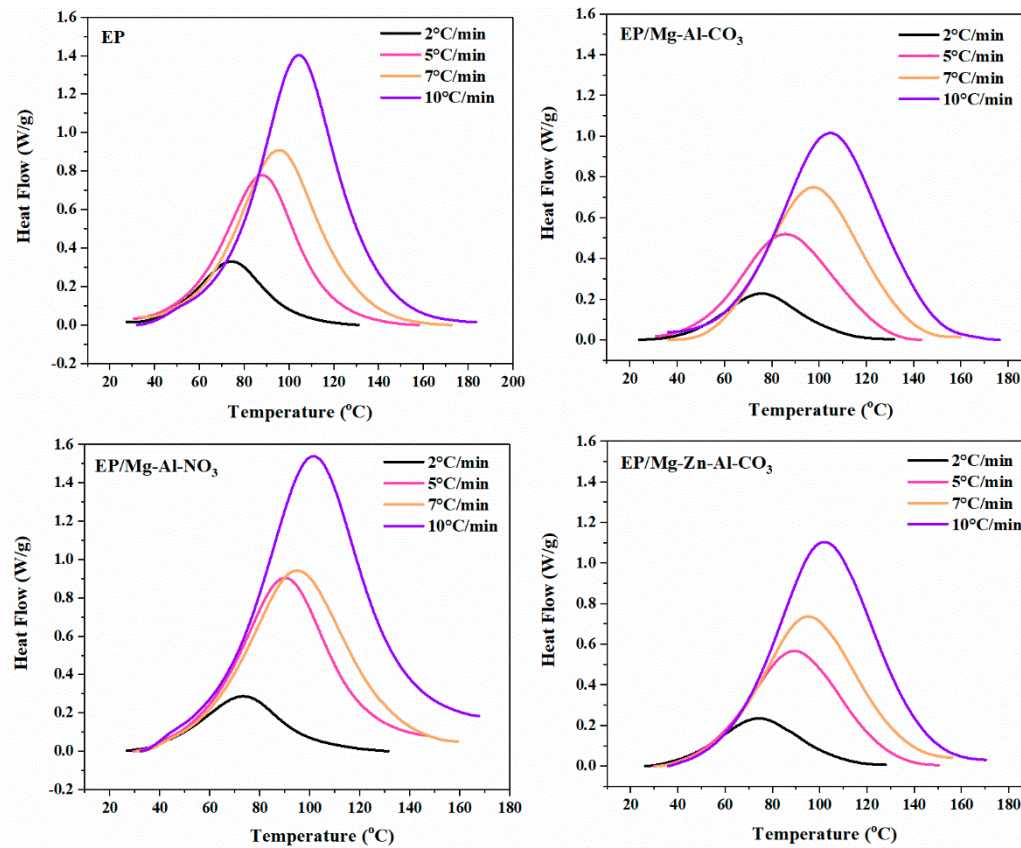


Figure 1. DSC thermograms of the neat epoxy (EP), EP/Mg-Al-CO₃, EP/Mg-Al-NO₃ and EP/Mg-Zn-Al-CO₃ nanocomposites at heating rates of 2, 5, 7 and 10 °C·min⁻¹.

The heat of cure increased directly by the extent of cure reaction (α), which can be obtained by the equation below:

$$\alpha = \frac{\Delta H_T}{\Delta H_\infty}, \tag{1}$$

In Equation (1), ΔH_∞ and ΔH_T are the total heat release during the cure reaction for the whole temperature range and the one up to temperature T , respectively. In Figure 2, the variation of fractional extent of cure reaction as a function of cure time was demonstrated for epoxy systems at heating rates of 2, 5, 7 and 10 °C·min⁻¹. As shown in Figure 2, the sigmoidal shape of the α -time curve is representative of the autocatalytic mechanism of cure reactions [33]. According to Figure 2, at β of 2 °C·min⁻¹, the introduction of Mg-Al-CO₃ restricted the access of curing agent molecules to the epoxide rings, thereby decelerating the cure reaction. Evidently, the time to reach $\alpha = 0.5$ was increased from 23.5 for the neat epoxy to 26.0 min for the nanocomposite. On the other hand, the incorporation of Mg-Al-NO₃ into the epoxy resin accelerated the cure reaction by the participation of nitrate ions in network formation, such that it decreased the time to reach $\alpha = 0.5$ from 23.5 min for the neat epoxy to 23.2 min for the nanocomposite [17]. In the case of EP/Mg-Zn-Al-CO₃, the Lewis acid effect of Zn²⁺ ions catalyzed the cure reaction. However, the low amount of Zn²⁺ released into the system was not sufficient to have a positive effect on the network formation, and evidently the time to reach $\alpha = 0.5$ increased from 23.5 min for the neat epoxy to 24.2 min for EP/Mg-Zn-Al-CO₃ [34]. At higher heating rates, the number of molecular interactions per unit volume in the system was increased,

which accelerated the cure reaction of the neat epoxy. For epoxy/LDH nanocomposites cured at a β of $7^\circ\text{C}\cdot\text{min}^{-1}$, the cure reaction was accelerated such that the time to reach $\alpha = 0.5$ decreased from 8.9 min for the neat epoxy to the 8.8 min for the EP/Mg-Zn-Al- CO_3 nanocomposite. Likewise, for the heating rate of $10^\circ\text{C}\cdot\text{min}^{-1}$ and for the epoxy nanocomposites containing Mg-Al- NO_3 or Mg-Zn-Al- CO_3 , the presence of nitrate and Zn^{2+} ions accelerated the cure reaction, as can be recognized by decrease in the time taken to reach $\alpha = 0.5$ from 7.2 min for the neat epoxy to 6.8 and 6.6 min for EP/Mg-Al- NO_3 and EP/Mg-Zn-Al- CO_3 , respectively. As per our experiences in the field, the partial cure of the epoxy/Mg-Al- CO_3 nanocomposite featured a shorter curing time compared to the epoxy resin [35].

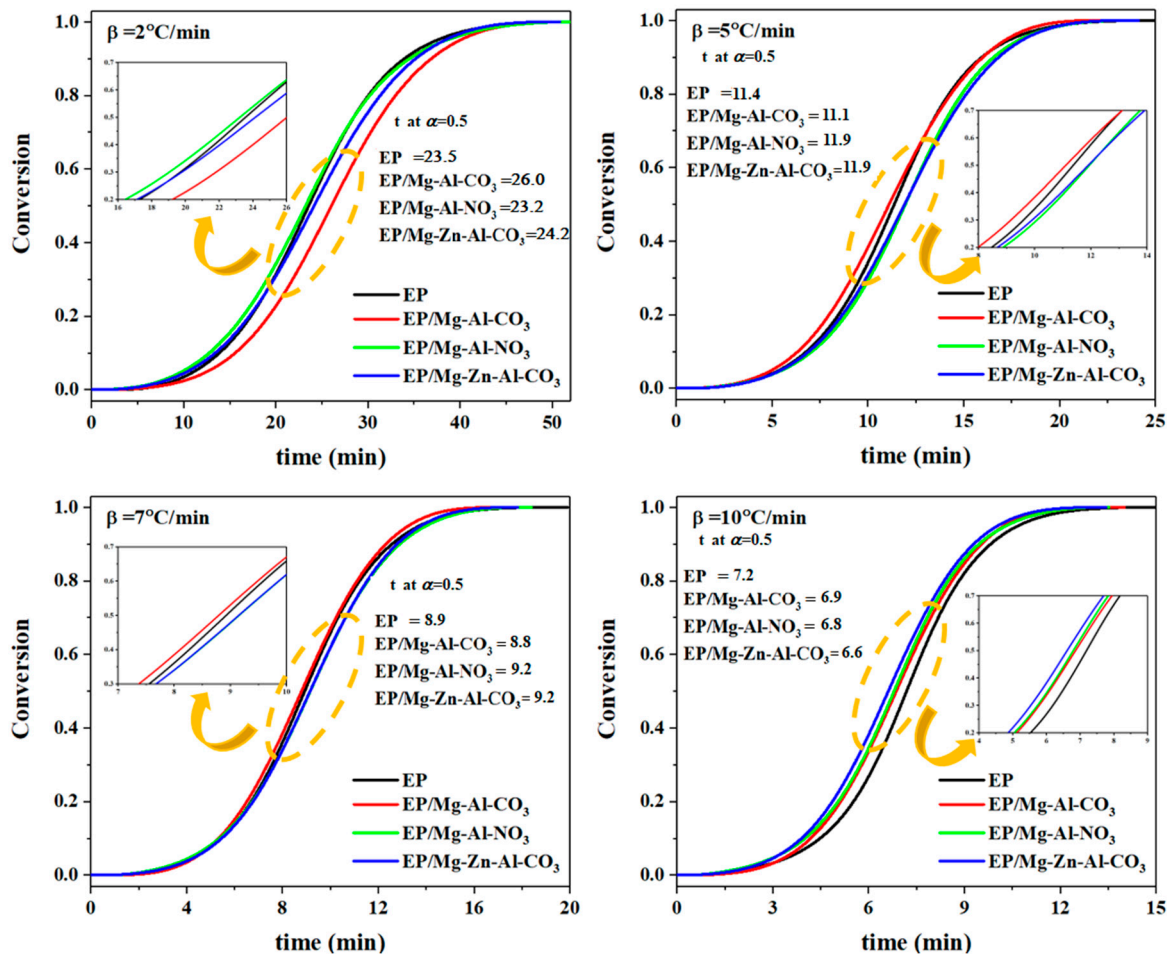


Figure 2. The fractional extent of conversion as a function of reaction time for EP, EP/Mg-Al- CO_3 , EP/Mg-Al- NO_3 and EP/Mg-Zn-Al- CO_3 nanocomposites at heating rates of 2, 5, 7 and $10^\circ\text{C}\cdot\text{min}^{-1}$.

3.2. Cure Kinetics Analysis

In isoconversional methods, such as the so-called model-free kinetics (MFK), it is a common assumption that the cure reaction rate at a given α is directly proportional to the cure temperature [36–38]. The well-known integral isoconversional methods of KAS and Flynn–Wall–Ozawa (FWO) and differential methods such as the *Friedman* model are used for determining the activation energy (E_a) of cure reaction [39,40]. In integral methods, due to the various formulations and approximations, the obtained E_a is different for various models. It is stated that differential methods are more accurate than the integral methods because no approximation is considered in developing the former. However, some inaccuracy is observed for such methods owing to difficulties in baseline selection or in reactions, which significantly depend on heating rate [23]. Thus, choosing the most accurate method has always been the subject of heated debate within the field of cure kinetics. In this work, both types of differential and integral kinetics methods are used for the analysis of non-isothermal

kinetics. Furthermore, the activation energy obtained from the *FWO* method is used as the first trial in the determination of the kinetics model by the *Málek* method to obtain a constant $E\alpha$ at various α . The information and fitting equations of the *Friedman* and *KAS* approaches are described mathematically and graphically in Appendices B.1 and B.2 of Appendix B, respectively. Figure 3 shows the variation of $E\alpha$ obtained from the *Friedman* and *KAS* models as a function of the extent of curing for the neat epoxy and its nanocomposites with Mg-Al-CO₃, Mg-Al-NO₃ and Mg-Zn-Al-CO₃ in the cure reaction interval of $0.1 < \alpha < 0.9$. As shown in Figure 3, the addition of Mg-Al-NO₃ and Mg-Zn-Al-CO₃ to the epoxy resin led to rise in $E\alpha$ with respect to neat epoxy, possibly due to the swelling of LDHs through intercalation with epoxy chains and the viscosity upturn [13], however, for the EP/Mg-Al-CO₃ nanocomposite, the $E\alpha$ decreased as a consequence of partially cured epoxy in the presence of the Mg-Al-CO₃ LDH [41,42]. Moreover, Figure 3 shows that the activation energy of the system decreased by the extent of cure reaction, especially at the early stage ($\alpha < 0.2$) of the *KAS* model, which is a sign of the autocatalytic nature of epoxy/amine reactions, in which the generation of hydroxyl groups assists in the ring opening of epoxy [43,44].

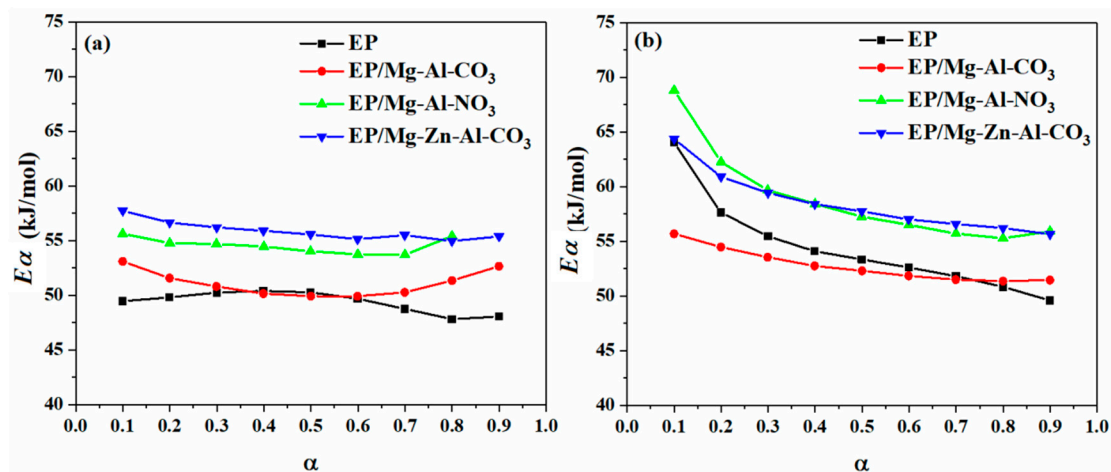


Figure 3. Variation of activation energy for EP, EP/Mg-Al-CO₃, EP/Mg-Al-NO₃ and EP/Mg-Zn-Al-CO₃ nanocomposites obtained by (a) differential *Friedman* and (b) integral *KAS* models.

The roles of Mg-Al-CO₃, Mg-Al-NO₃ and Mg-Zn-Al-CO₃ in the cure reaction of the epoxy/amine system are schematically shown in Figure 4. As can be seen in Figure 4, Mg-Al-CO₃ cannot take part in epoxide ring-opening reaction due to the strong hydrogen bonding of three oxygen atoms of intercalated carbonate ions with the hydroxyl groups of the LDH layers due to the horizontal orientation of CO₃²⁻ within the LDH layers [30,31]. On the contrary, the nitrate anion plays a different role in cure reactions due to its different configuration compared to the carbonate anion [32]. In NO₃⁻, two oxygen atoms are located near the OH groups of one layer and the third one closer to the opposite side. Thus, this configuration causes a limited interaction between the nitrate anions and hydroxyl groups, while this increases the chances of interactions between the intercalated water molecules and LDH layers [45]. Because of the weak interaction of NO₃⁻ with hydroxide layers, nitrate anions can attack the C-O bond in the epoxide, leading to ring-opening reactions that facilitate the curing of the EP/Mg-Al-NO₃ nanocomposite [17]. In the case of EP/Mg-Zn-Al-CO₃, by catching the oxygens' lone-pair electron in the epoxide rings by the Lewis acid effect of Zn²⁺, the epoxide ring-opening reaction was influenced by Zn²⁺. On the other hand, due to the low concentration of released ions, the positive effect of Zn²⁺ on the crosslinking was not observed [34].

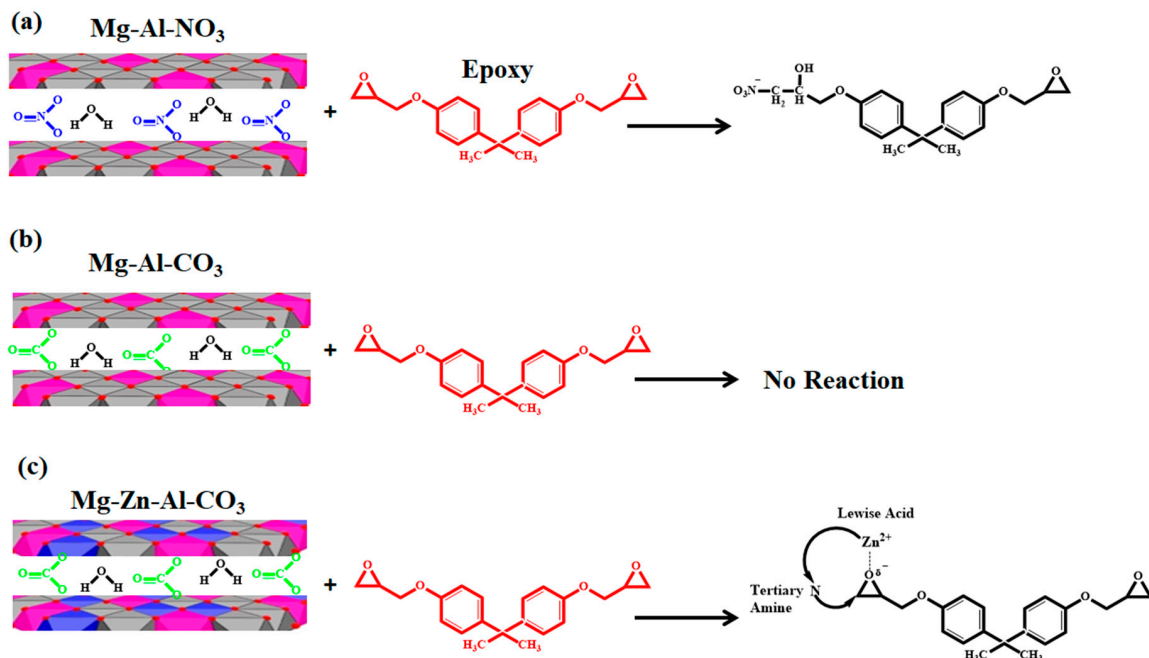


Figure 4. Possible reactions between (a) Mg-Al-NO₃, (b) Mg-Al-CO₃ and (c) Mg-Zn-Al-CO₃ with epoxy resin.

3.2.1. Determining the Reaction Model and the Order of Reaction

It is necessary to determine the reaction model in order to clarify the cure mechanism of the epoxy/amine system in the presence of LDH nanosheets. The *Friedman* and *Málek* methods are useful for knowing whether or not the autocatalytic cure mechanism is dominant. From the *Friedman* curve, the curing mechanism was determined by Equation (A3) in Appendix C.1 of Appendix C. As the maximum point of α in Figure A3 is located in the range of 0.2–0.4, the mechanism of reaction in the epoxy/LDH nanocomposites was found to be autocatalytic [46,47]. The kinetic model was designated by the maximum points of $y(\alpha) = (\alpha_m)$, $z(\alpha) = (\alpha_p^\infty)$ and the peak of conversion in the DSC curves (α_p) based on the *Málek* method (see the Appendix C.2 of Appendix C). The values of α_m , α_p and α_p^∞ for the epoxy/amine systems at different heating rates are listed in Table 1. Accordingly, the values of α_m are lower than those of α_p^∞ and, at the same time, $\alpha_p < 0.633$, suggesting a two-parameter autocatalytic kinetic model for all studied systems [48,49].

Since the autocatalytic cure mechanism was confirmed for the EP, EP/Mg-Al-CO₃, EP/Mg-Al-NO₃ and EP/Mg-Zn-Al-CO₃ systems by the *Friedman* and *Málek* models, the following equation was used:

$$\frac{da}{dt} = A \exp\left(-\frac{E_\alpha}{RT}\right) \alpha^m (1-p)^n, \quad (2)$$

where n , m and A are the degrees of autocatalytic and non-catalytic reactions and the frequency factor, respectively. The values of m , n and $\ln A$ are determined from Equations (A11) and (A12) in Appendix D.

Table 1. The values of α_p , α_m and α_p^∞ obtained from the *Málek* model at various heating rates.

Designation	Heating Rate (°C·min ⁻¹)	α_p^∞	α_m	α_p
EP	2	0.493	0.199	0.519
	5	0.489	0.182	0.544
	7	0.481	0.186	0.529
	10	0.561	0.215	0.532
EP/Mg-Al-CO ₃	2	0.496	0.179	0.529
	5	0.513	0.149	0.523
	7	0.536	0.147	0.531
	10	0.516	0.137	0.537
EP/Mg-Al-NO ₃	2	0.502	0.134	0.531
	5	0.684	0.136	0.546
	7	0.648	0.095	0.530
	10	0.668	0.009	0.545
EP/Mg-Zn-Al-CO ₃	2	0.494	0.122	0.527
	5	0.544	0.092	0.532
	7	0.592	0.095	0.532
	10	0.536	0.092	0.533

The E_a value is the average amount over the whole range of α based on the *Friedman* and *KAS* methods (Table 2). For the EP/Mg-Al-CO₃ system, lower values of the apparent activation energy can be assigned to the incomplete curing, which arose from limited interaction.

Table 2. The kinetic parameters obtained for the curing of the prepared samples based on the *Friedman* and *KAS* methods at different heating rates.

Designation	Heating Rate (°C·min ⁻¹)	\bar{E}_a (kJ/mol)	$\ln(A)$ (1/s)	Mean (1/s)	m	Mean	n	Mean
<i>Friedman</i> method								
EP	2	49.38	15.44	15.53	0.437	0.441	1.406	1.426
	5		15.64		0.446		1.410	
	7		15.48		0.390		1.422	
	10		15.55		0.491		1.465	
EP/Mg-Al-CO ₃	2	51.07	15.73	15.70	0.313	0.231	1.327	1.27
	5		15.83		0.189		1.259	
	7		15.63		0.205		1.230	
	10		15.63		0.216		1.265	
EP/Mg-Al-NO ₃	2	55.08	17.44	17.31	0.348	0.300	1.527	1.436
	5		17.30		0.324		1.380	
	7		17.19		0.228		1.396	
	10		17.33		0.298		1.440	
EP/Mg-Zn-Al-CO ₃	2	55.88	17.36	17.33	0.206	0.176	1.345	1.329
	5		17.30		0.158		1.310	
	7		17.33		0.169		1.321	
	10		17.32		0.172		1.341	
<i>KAS</i> method								
EP	2	54.37	17.16	17.17	0.389	0.386	1.450	1.469
	5		17.29		0.391		1.452	
	7		17.10		0.335		1.468	
	10		17.13		0.430		1.507	

Table 2. Cont.

Designation	Heating Rate (°C·min ⁻¹)	$\bar{E}\alpha$ (kJ/mol)	$\ln(A)$ (1/s)	Mean (1/s)	m	Mean	n	Mean
EP/Mg-Al-CO ₃	2	52.76	16.31	16.26	0.295	0.212	1.342	1.285
	5		16.39		0.169		1.275	
	7		16.17		0.187		1.245	
	10		16.17		0.195		1.280	
EP/Mg-Al-NO ₃	2	58.86	18.75	18.56	0.309	0.254	1.562	1.468
	5		18.54		0.279		1.410	
	7		18.41		0.181		1.430	
	10		18.54		0.248		1.472	
EP/Mg-Zn-Al-CO ₃	2	58.47	18.25	18.18	0.178	0.145	1.368	1.352
	5		18.15		0.127		1.333	
	7		18.17		0.137		1.344	
	10		18.14		0.140		1.364	

By comparing the results in Table 2, the summation of the degrees of the autocatalytic and non-catalytic reactions ($m + n$), which is the overall order of the cure reaction, is more than one, which explains the complexity of the epoxy/amine cure reaction [50]. Furthermore, the autocatalytic reaction order (m) is lower for the epoxy/LDH nanocomposites compared to the neat epoxy, suggesting a shift in the curing mechanism from autocatalytic to non-catalytic reactions [51]. On the other hand, increasing the frequency factor for EP/Mg-Al-NO₃ is indicative of enhanced interaction due to the participation of nitrate anions in the epoxide ring-opening reaction [52]. For the EP/Mg-Zn-Al-CO₃ nanocomposite, however, despite increased interactions, due to the low concentration of Zn²⁺ ions in the system, no positive role in improving the cure reaction was detected.

3.2.2. Model Validation

As a final step, for the validation of the kinetics parameters obtained from previous steps, the curing rate was calculated and compared with the experimental curve. Figure 5 compares the curing rate for neat epoxy and the EP/Mg-Al-CO₃, EP/Mg-Al-NO₃ and EP/Mg-Zn-Al-CO₃ nanocomposites, respectively, obtained by the analytical models (*Friedman* and *KAS* models) with the experimental values. It is observed that both isoconversional methods satisfactorily match with the experimental data [53]. At a late stage of cure ($\alpha > 0.8$), however, some deviation from the experimental data was observed, possibly due to the fact that isoconversional methods cannot predict vitrification. Therefore, in the early stages of curing, the reaction progress in the liquid phase, and thus the reaction, is controlled chemically before the gelation and vitrification phenomena, where it is controlled by diffusion [54].

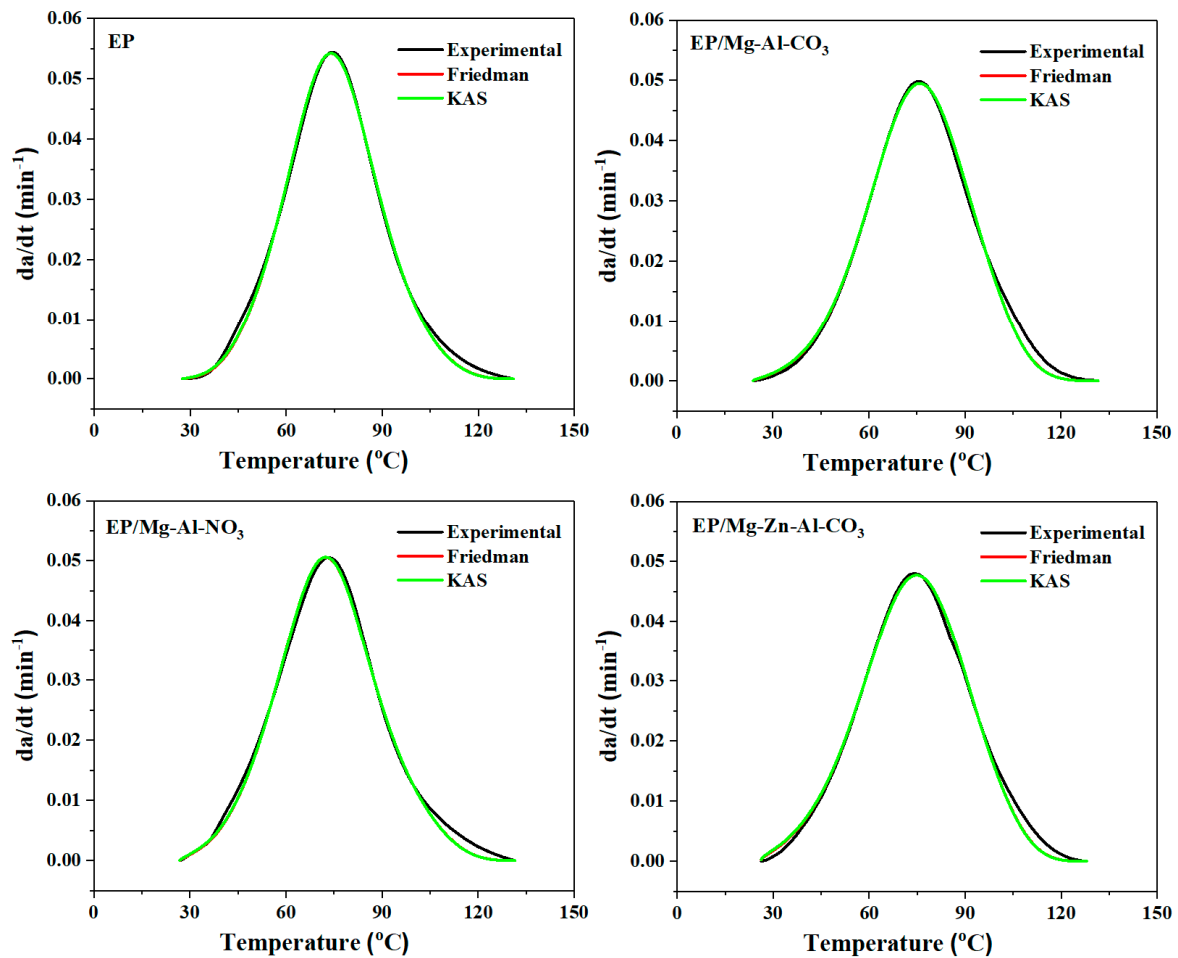


Figure 5. Comparison of experimental data with the kinetic models (*Friedman* and *KAS*) for prepared samples at a heating rate of 2 °C·min⁻¹.

4. Conclusions

Generally, the evaluation of the cure kinetics of epoxy/Mg-Al LDH nanocomposites elucidates that the LDH nanosheets significantly affect the crosslinking in the epoxy resin, while the curing mechanism of epoxy/LDH systems remains unchanged. The calculation of the activation energy by both differential *Friedman* and integral *KAS* methods suggests that the incorporation of Mg-Al-NO₃ and Mg-Zn-Al-CO₃ increased the energy needed for network formation, possibly due to the viscosity upturn and perturbed cure reaction with respect to the neat epoxy. The average values of $E\alpha$ obtained by different methods are compared in Table 3. An increase in the activation energy of the epoxy/LDH nanocomposites with respect to the neat epoxy is possibly due to the swelling of the LDHs through intercalation with epoxy chains or increased viscosity. However, reduction in the activation energy of the epoxy/Mg-Al-CO₃ nanocomposite can be ascribed to the partial cure of the epoxy nanocomposite in the presence of the Mg-Al-CO₃ LDH.

Table 3. The kinetic parameters obtained for the studied systems.

Sample Code	Cure State	$\bar{E}\alpha$ (kJ/mol) (<i>Friedman</i>)	$\bar{E}\alpha$ (kJ/mol) (<i>KAS</i>)	$E\alpha$ (kJ/mol) (<i>FWO</i>)
EP	-	49.38	54.37	55.74
EP/Mg-Al-CO ₃	Poor	51.07	52.76	54.60
EP/Mg-Al-NO ₃	Excellent	55.08	58.86	58.47
EP/Mg-Zn-Al-CO ₃	Poor	55.88	58.47	60.59

The enhancement of the frequency factor as a criterion of the number of molecular interactions for the EP/Mg-Al-NO₃ system compared to the neat epoxy (from 15.53 to 17.31 s⁻¹ by the *Friedman* method and from 17.17 to 18.56 s⁻¹ by the *KAS* method) elucidates the improvement of the curability of epoxy/LDH nanocomposites by the participation of nitrate anions in epoxide ring-opening reactions. In the case of the EP/Mg-Zn-Al-CO₃ nanocomposite, however, the trace of Zn²⁺ ions in the system neutralized the positive effect due to enhanced molecular interactions detected by a frequency factor increase.

Author Contributions: Conceptualization, M.R.S.; methodology, S.M.R.P.; software, Z.K.; validation, P.V.P. and M.J.; formal analysis, A.E.; investigation, S.H.; writing—original draft preparation, Z.K.; writing—review and editing, P.V.P.; visualization, M.R.G. and F.J.S.; supervision, M.R.S. All authors have read and agreed to the published version of the manuscript.

Funding: This research received no external funding.

Conflicts of Interest: The authors declare no conflict of interest. The funders had no role in the design of the study; in the collection, analyses, or interpretation of data; in the writing of the manuscript, or in the decision to publish the results.

Appendix A. Materials and Methods

Appendix A.1. Materials

Epoxy resin (epoxide equivalent weight (EEW): 174 g/eq) and triethylenetetramine (TETA) as a curing agent were provided by Sigma Aldrich (Italy, Milano). Moreover, chloroform was acquired from Sigma-Aldrich (99% purification).

Appendix A.2. Preparation of Epoxy Nanocomposites

Mg-Al-CO₃, Mg-Al-NO₃ and Mg-Zn-Al-CO₃ LDHs were synthesized according to previous studies [30–32]. Synthesized LDHs (0.1 wt.%) were added to epoxy resin to prepare the EP/Mg-Al-CO₃, EP/Mg-Al-NO₃ and EP/Mg-Zn-Al-CO₃ nanocomposites through the solution method. The LDH nanosheets were dispersed into the chloroform by sonication with 40% power for 30 min in an ice bath, then immediately added to the epoxy resin and mixed with a magnetic stirrer to remove the solvent for a week at room temperature. Finally, the stoichiometric content of TETA (100:14) was added to the epoxy system and carefully mixed.

Appendix A.3. Characterization of Epoxy Nanocomposites

The cure reaction of the epoxy/amine system in the presence of 0.1 wt.% of the Mg-Al-CO₃, Mg-Al-NO₃ and Mg-Zn-Al-CO₃ LDHs was studied non-isothermally using a differential scanning calorimeter (DSC Q200 model, TA Instrument, New Castle, DE, USA). DSC analysis was performed at heating rates (β) of 2, 5, 7 and 10 °C·min⁻¹ in the temperature range of -50 to 250 °C in a nitrogen atmosphere with flow rates of 50 mL·min⁻¹.

Appendix B. Isoconversional Kinetic Methods

Appendix B.1. Friedman Model

Friedman model is defined based on the following equation [33,55]:

$$\ln \left[\beta_i \left(\frac{d\alpha}{dT} \right)_{\alpha,i} \right] = \ln [f(\alpha)A_\alpha] - \frac{E_\alpha}{RT_{\alpha,i}}, \quad (\text{A1})$$

By plotting $\ln \left[\beta_i (d\alpha/dT)_{\alpha,i} \right]$ vs. $1/T\alpha$, the value of activation energy (E_α) in each α can be obtained from the slope of Figure A1.

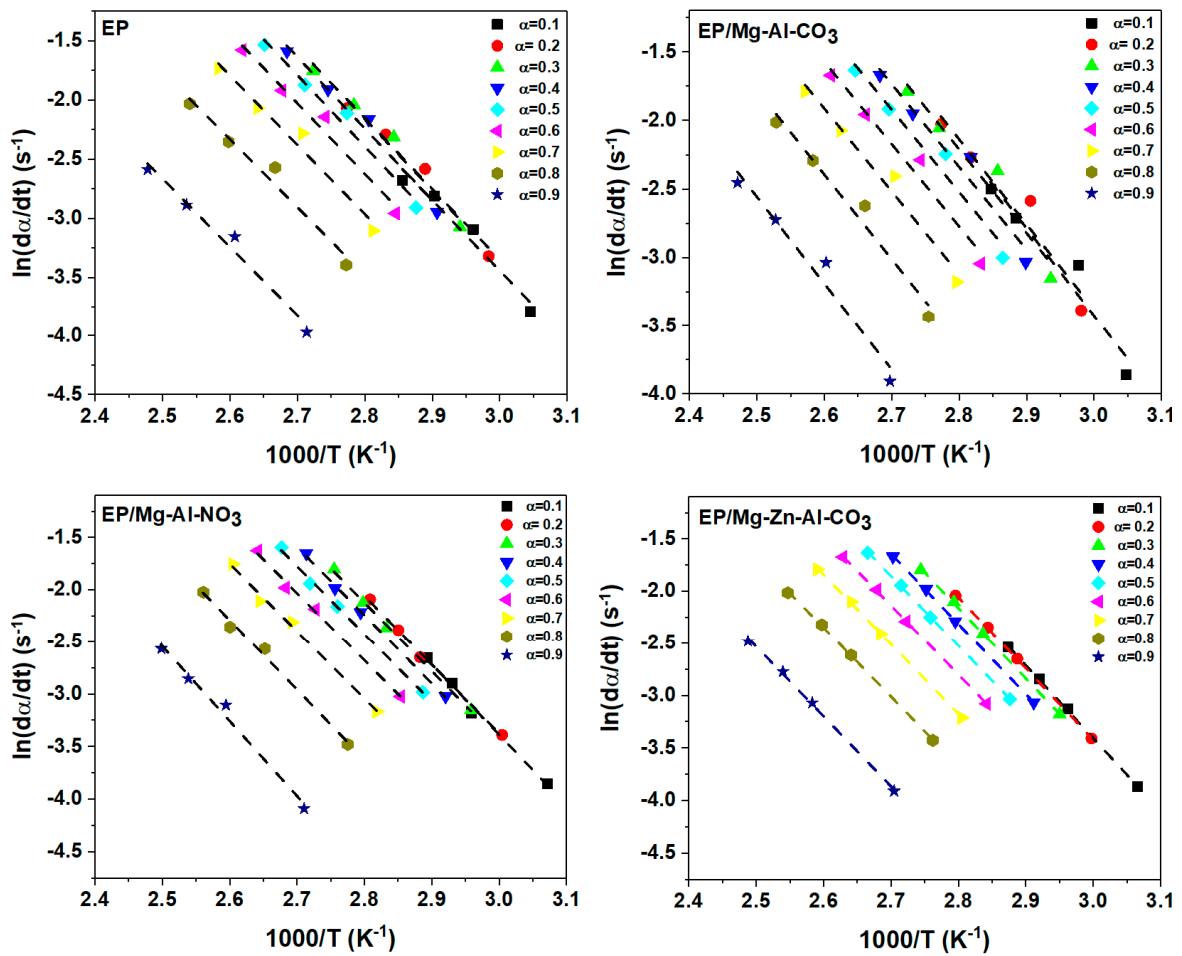


Figure A1. Plots of $\ln(d\alpha/dt)$ vs. $1/T$ for the prepared samples based on the Friedman model at $\beta = 2 \text{ }^\circ\text{C}\cdot\text{min}^{-1}$.

Appendix B.2. KAS Method

KAS method is defined by the following equation [56,57]:

$$\ln\left(\frac{\beta_i}{T_{\alpha,i}^{1.92}}\right) = \text{Const} - 1.0008\left(\frac{E_\alpha}{RT_\alpha}\right), \tag{A2}$$

Plotting $\ln(\beta_i/T_{\alpha,i}^{1.92})$ vs. $1/T_\alpha$ gives a straight line; its slope gives the activation energy (Figure A2).

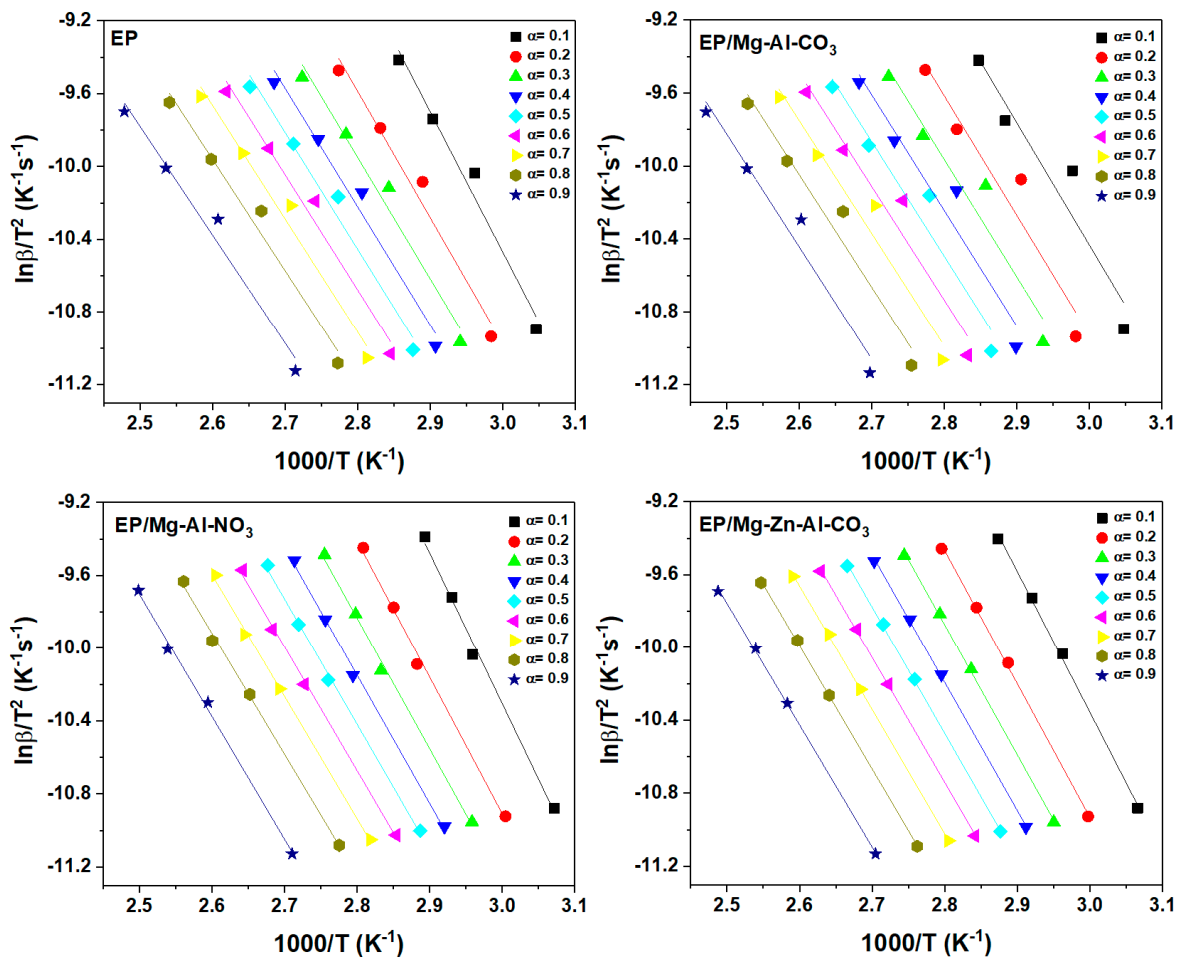


Figure A2. Plots of $\ln(\beta/T^{1.92})$ vs. $1/T$ for the prepared samples based on the KAS model.

Appendix C. Selection of the Cure Reaction Model

Appendix C.1. Friedman Model

Based on the *Friedman* method, the model of the epoxy cure reaction can be determined using Equation (A3). The shape of the plot of $\ln[Af(\alpha)]$ vs. $\ln(1 - \alpha)$ denotes the deviation from the n th order reaction (Figure A3) [58].

$$\ln[Af(\alpha)] = \ln\left(\frac{d\alpha}{dt}\right) + \frac{E_\alpha}{RT} = \ln A + n \ln(1 - \alpha), \quad (A3)$$

For the n th order cure mechanism, a straight line was obtained by plotting $\ln[Af(\alpha)]$ vs. $\ln(1 - \alpha)$, whose slope gives the reaction degree (n).

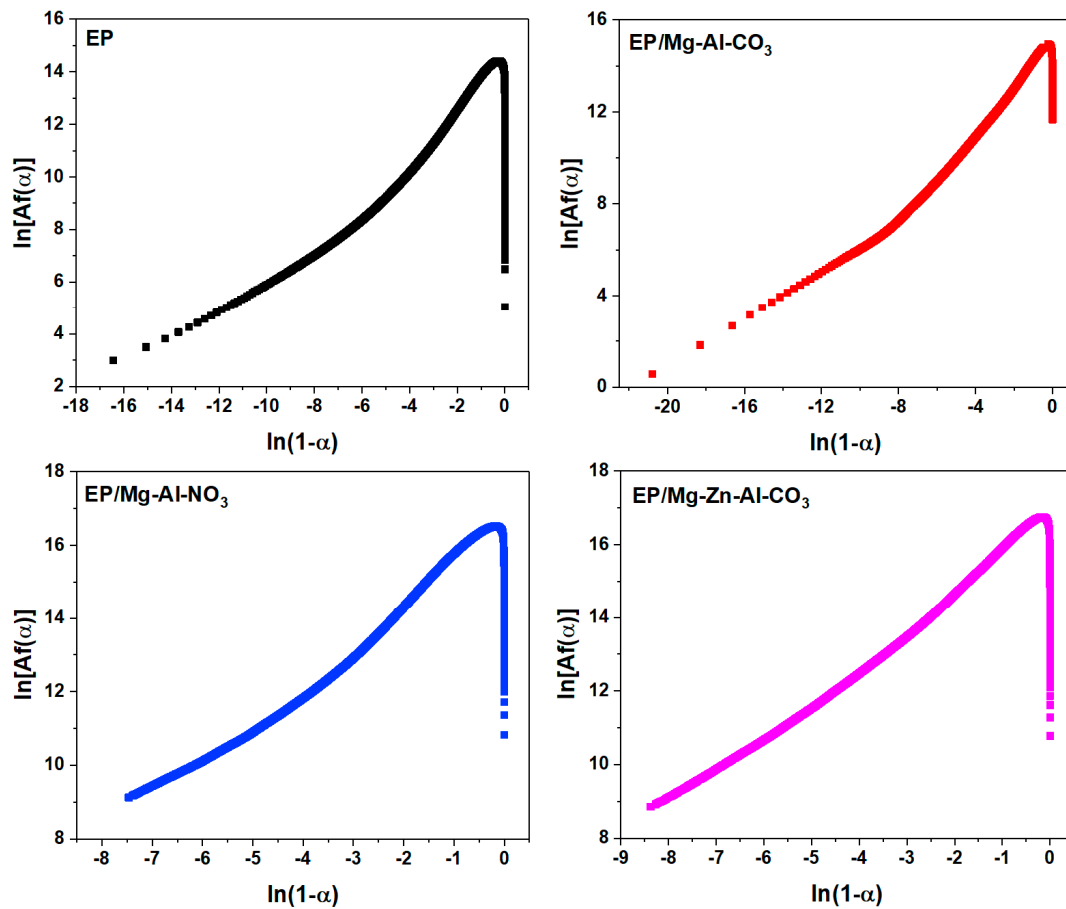


Figure A3. Plots of $\ln [Af(\alpha)]$ vs. $\ln(1 - \alpha)$ for the samples under a heating rate of $2\text{ }^\circ\text{C}\cdot\text{min}^{-1}$ used in the calculation of activation energy via the *Friedman* method.

Appendix C.2. Málek Method

The kinetic model based on the Málek method is determined using the following equations:

$$y(\alpha) = \left(\frac{d\alpha}{dt}\right)_\alpha \exp\left(\frac{E_\alpha}{RT_\alpha}\right) = Af(\alpha), \tag{A4}$$

$$z(\alpha) = \left(\frac{d\alpha}{dt}\right)_\alpha T_\alpha^2 \left[\frac{\pi(x)}{\beta T_\alpha}\right], \tag{A5}$$

The term in the brackets of Equation (A5) has no significant effect on the shape of the $z(\alpha)$ function and can be omitted. In Equation (A4), the amount of E_0 is determined by the *FWO* method, where the change in the activation energy with the variation of α remains constant, from the following equation [59,60]:

$$\ln(\beta_i) = \text{Const} - 1.052\left(\frac{E_\alpha}{RT_\alpha}\right) \tag{A6}$$

In the *FWO* method, the activation energy is determined from the slope of $\ln(\beta_i)$ vs. $1/T$, as shown in Figure A4. This method gives the activation energy depending on conversion. By the *FWO* method, the values of activation energy are obtained as 55.74 kJ/mol, 54.60 kJ/mol, 58.47 kJ/mol and 60.59 kJ/mol for neat epoxy, EP/Mg-Al-CO₃, EP/Mg-Al-NO₃ and EP/Mg-Zn-Al-CO₃, respectively.

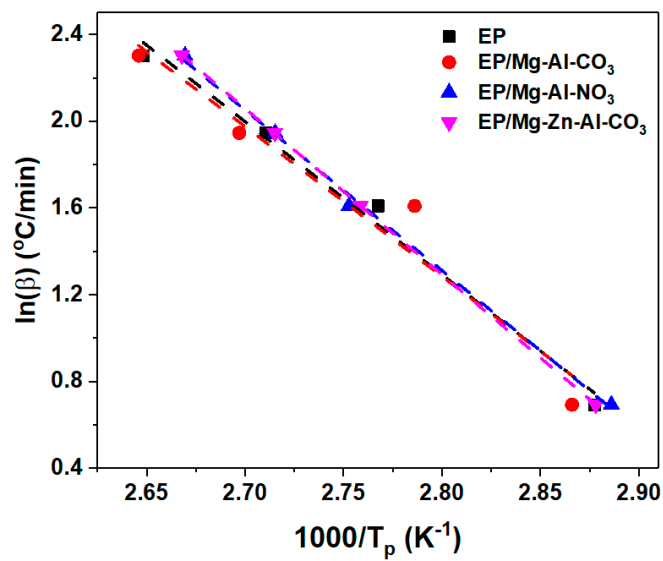


Figure A4. Plots of $\ln(\beta)$ vs. $1/T$ for epoxy resin and prepared nanocomposites derived from the FWO model.

The experimental values of $y(\alpha)$ and $z(\alpha)$ for the EP, EP/Mg-Al-CO₃, EP/Mg-Al-NO₃ and EP/Mg-Zn-Al-CO₃ nanocomposites as a function of conversion are shown in Figure A5 and compared with theoretical master plots.

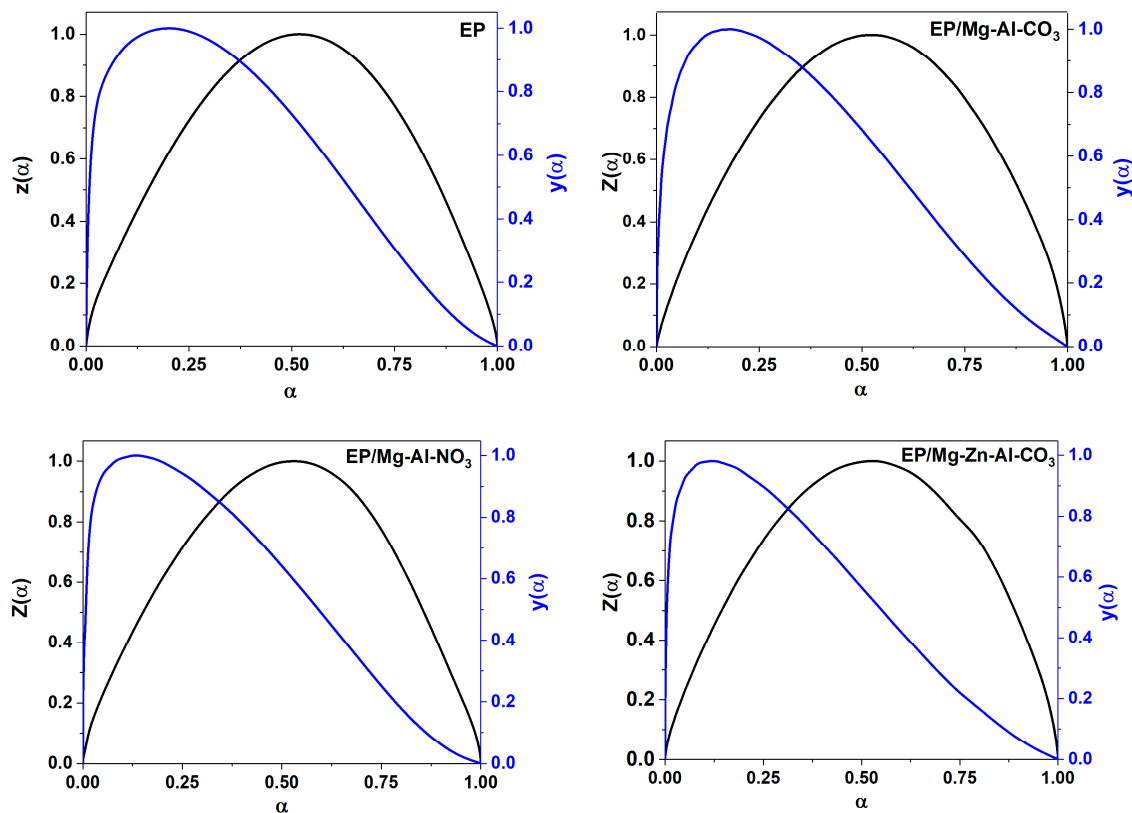


Figure A5. Variation of $y(\alpha)$ and $z(\alpha)$ versus conversion for the prepared samples based on the Malek model.

Then $y(\alpha)$ and $z(\alpha)$ were normalized as follows to vary between 0 and 1:

$$y_n(\alpha) = \frac{y(\alpha)}{\max[y(\alpha)]}, \tag{A7}$$

$$z_n(\alpha) = \frac{z(\alpha)}{\max[z(\alpha)]}, \tag{A8}$$

The maximum values, $\max[y(\alpha)] = \alpha_m$ and $\max[z(\alpha)] = \alpha_p$, can be found from the following expressions:

$$f'(\alpha_m) = 0, \tag{A9}$$

$$f'(\alpha_p) g(\alpha_p) = -1, \tag{A10}$$

Appendix D. Determination of the Degree of Reaction

The degrees of autocatalytic reaction (n and m) and the frequency factor (A) can be determined through the following equations [61,62]:

$$\text{Value I} = \ln\left(\frac{d\alpha}{dt}\right) + \frac{E_a}{RT} - \ln\left[\frac{d(1-\alpha)}{dt}\right] - \frac{E_a}{RT'} = (n-m) \ln\left(\frac{1-\alpha}{\alpha}\right), \tag{A11}$$

$$\text{Value II} = \ln\left(\frac{d\alpha}{dt}\right) + \frac{E_a}{RT} + \ln\left[\frac{d(1-\alpha)}{dt}\right] + \frac{E_a}{RT'} = (n+m) \ln(\alpha - \alpha^2) + 2 \ln A, \tag{A12}$$

The slope of the plot of Value I vs. $\ln[(1-\alpha)/\alpha]$ (Figure A6) gives the value of $(n-m)$, and the slope and intercept of the plot of Value II vs. $\ln(\alpha - \alpha^2)$ (Figure A7) give the value of $(n+m)$ and $2 \ln A$.

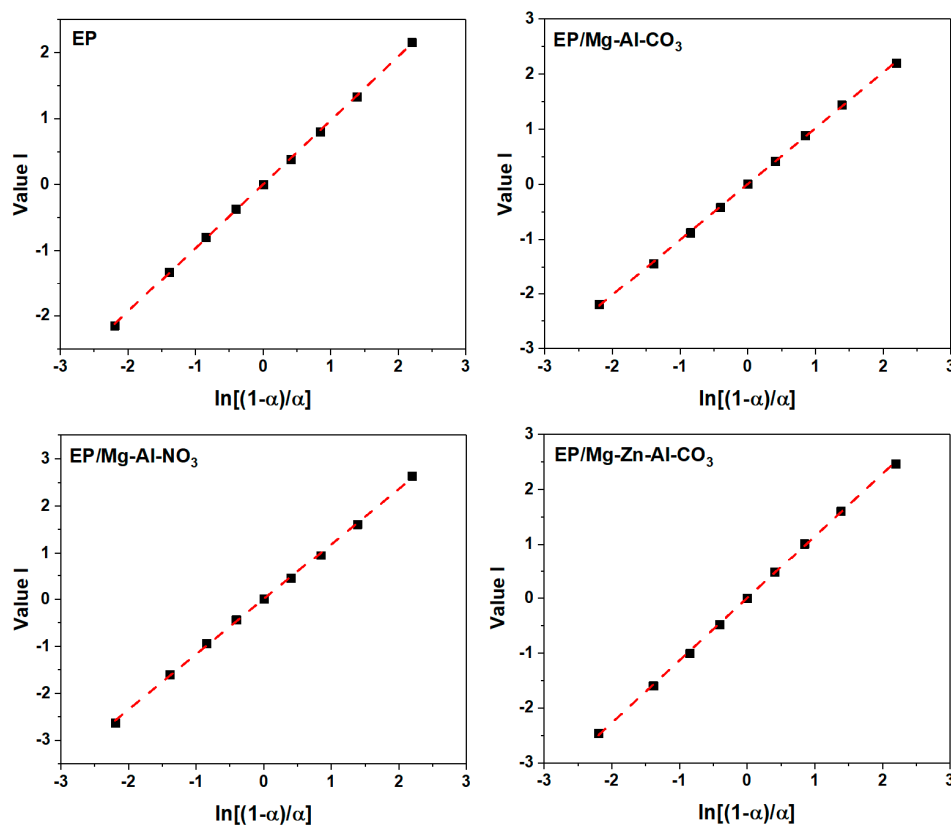


Figure A6. Plots of value I calculated using DSC data for the prepared epoxy system under a heating rate of $2\text{ }^{\circ}\text{C}\cdot\text{min}^{-1}$.

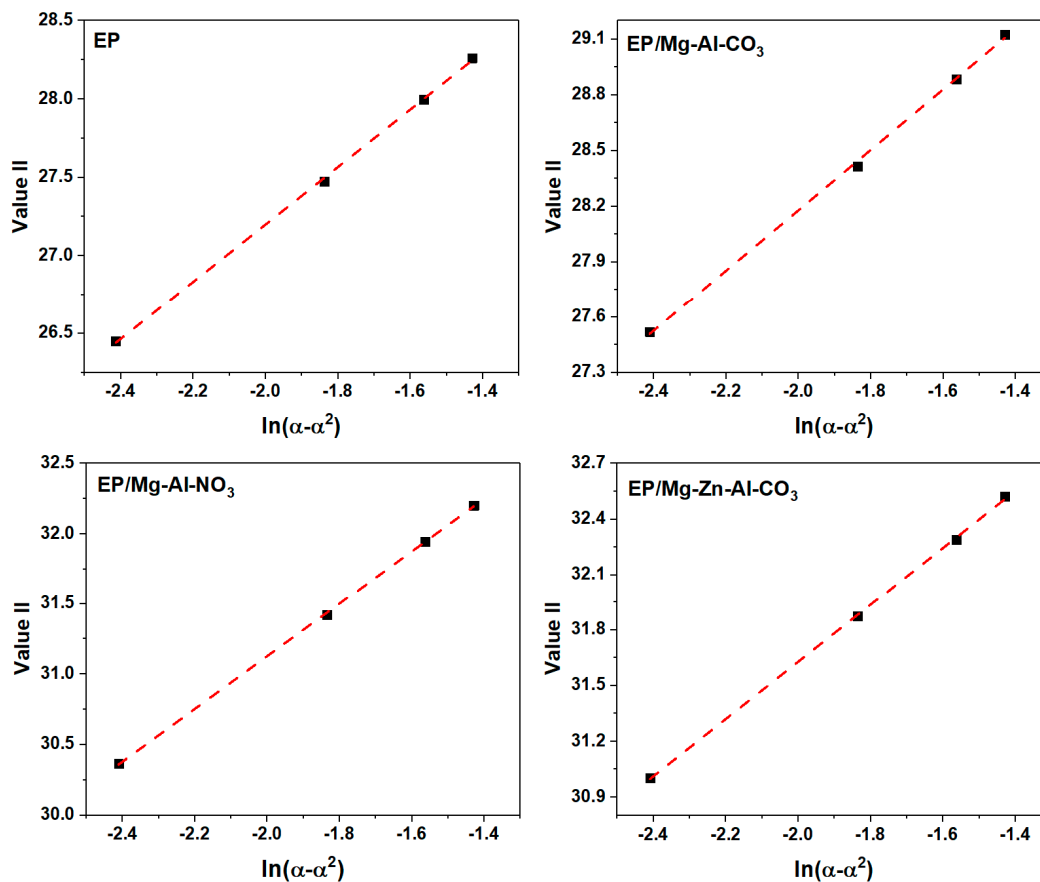


Figure A7. Plots of Value II calculated for the prepared samples under a heating rate of $2\text{ }^{\circ}\text{C}\cdot\text{min}^{-1}$.

References

- Schaming, D.; Remita, H. Nanotechnology: From the ancient time to nowadays. *Found. Chem.* **2015**, *17*, 187–205. [\[CrossRef\]](#)
- Chatterjee, A.; Bharadiya, P.; Hansora, D. Layered double hydroxide based bionanocomposites. *Appl. Clay Sci.* **2019**, *177*, 19–36. [\[CrossRef\]](#)
- Zümreoglu-Karan, B.; Ay, A. Layered double hydroxides—Multifunctional nanomaterials. *Chem. Pap.* **2012**, *66*, 1–10. [\[CrossRef\]](#)
- Wu, M.; Wu, J.; Zhang, J.; Chen, H.; Zhou, J.; Qian, G.; Xu, Z.; Du, Z.; Rao, Q. A review on fabricating heterostructures from layered double hydroxides for enhanced photocatalytic activities. *Catal. Sci. Technol.* **2018**, *8*, 1207–1228. [\[CrossRef\]](#)
- Qu, J.; Zhang, Q.; Li, X.; He, X.; Song, S. Mechanochemical approaches to synthesize layered double hydroxides: A review. *Appl. Clay Sci.* **2016**, *119*, 185–192. [\[CrossRef\]](#)
- Benício, L.P.F.; Silva, R.A.; Lopes, J.A.; Eulálio, D.; Santos, R.M.M.; Aquino, L.A.; Vergütz, L.; Novais, R.F.; Costa, L.M.; Pinto, F.G. Layered double hydroxides: Nanomaterials for applications in agriculture. *Rev. Bras. Ciênc. Solo* **2015**, *39*, 1–13. [\[CrossRef\]](#)
- Leroux, F.; Besse, J.-P. Polymer interleaved layered double hydroxide: A new emerging class of nanocomposites. *Chem. Mater.* **2001**, *13*, 3507–3515. [\[CrossRef\]](#)
- Chhetri, S.; Samanta, P.; Murmu, N.C.; Kuila, T. Anticorrosion Properties of Epoxy Composite Coating Reinforced by Molybdate-Intercalated Functionalized Layered Double Hydroxide. *J. Compos. Sci.* **2019**, *3*, 11. [\[CrossRef\]](#)
- Becker, C.M.; Gabbardo, A.D.; Wypych, F.; Amico, S.C. Mechanical and flame-retardant properties of epoxy/Mg–Al LDH composites. *Compos. Part A Appl. Sci. Manuf.* **2011**, *42*, 196–202. [\[CrossRef\]](#)

10. Jouyandeh, M.; Ganjali, M.R.; Ali, J.A.; Aghazadeh, M.; Stadler, F.J.; Saeb, M.R. Curing epoxy with electrochemically synthesized $\text{Ni}_x\text{Fe}_3\text{-xO}_4$ magnetic nanoparticles. *Prog. Org. Coat.* **2019**, *136*, 105198. [[CrossRef](#)]
11. Jouyandeh, M.; Tikhani, F.; Hampp, N.; Akbarzadeh Yazdi, D.; Zarrintaj, P.; Reza Ganjali, M.; Reza Saeb, M. Highly curable self-healing vitrimer-like cellulose-modified halloysite nanotube/epoxy nanocomposite coatings. *Chem. Eng. J.* **2020**, *396*, 125196. [[CrossRef](#)]
12. Jouyandeh, M.; Ali, J.A.; Aghazadeh, M.; Formela, K.; Saeb, M.R.; Ranjbar, Z.; Ganjali, M.R. Curing epoxy with electrochemically synthesized $\text{Zn}_x\text{Fe}_3\text{-xO}_4$ magnetic nanoparticles. *Prog. Org. Coat.* **2019**, *136*, 105246. [[CrossRef](#)]
13. Tomić, M.; Dunjić, B.; Nikolić, M.S.; Maletaškić, J.; Pavlović, V.B.; Bajat, J.; Djonlagić, J. Dispersion efficiency of montmorillonites in epoxy nanocomposites using solution intercalation and direct mixing methods. *Appl. Clay Sci.* **2018**, *154*, 52–63. [[CrossRef](#)]
14. Zuo, J.; Li, H.; Dong, B.; Wang, L. Effects of metakaolin on the mechanical and anticorrosion properties of epoxy emulsion cement mortar. *Appl. Clay Sci.* **2020**, *186*, 105431. [[CrossRef](#)]
15. Bayat, S.; Moini Jazani, O.; Molla-Abbasi, P.; Jouyandeh, M.; Saeb, M.R. Thin films of epoxy adhesives containing recycled polymers and graphene oxide nanoflakes for metal/polymer composite interface. *Prog. Org. Coat.* **2019**, *136*, 105201. [[CrossRef](#)]
16. Jouyandeh, M.; Jazani, O.M.; Navarchian, A.H.; Shabaniyan, M.; Vahabi, H.; Saeb, M.R. Bushy-surface hybrid nanoparticles for developing epoxy superadhesives. *Appl. Surf. Sci.* **2019**, *479*, 1148–1160. [[CrossRef](#)]
17. Karami, Z.; Jouyandeh, M.; Ali, J.A.; Ganjali, M.R.; Aghazadeh, M.; Maadani, M.; Rallini, M.; Luzi, F.; Torre, L.; Puglia, D.; et al. Cure Index for labeling curing potential of epoxy/LDH nanocomposites: A case study on nitrate anion intercalated Ni-Al-LDH. *Prog. Org. Coat.* **2019**, *136*, 105228. [[CrossRef](#)]
18. Jouyandeh, M.; Ganjali, M.R.; Ali, J.A.; Akbari, V.; Karami, Z.; Aghazadeh, M.; Zarrintaj, P.; Saeb, M.R. Curing epoxy with polyethylene glycol (PEG) surface-functionalized $\text{Gd}_x\text{Fe}_3\text{-xO}_4$ magnetic nanoparticles. *Prog. Org. Coat.* **2019**, *137*, 105283. [[CrossRef](#)]
19. Jouyandeh, M.; Rahmati, N.; Movahedifar, E.; Hadavand, B.S.; Karami, Z.; Ghaffari, M.; Taheri, P.; Bakhshandeh, E.; Vahabi, H.; Ganjali, M.R.; et al. Properties of nano- Fe_3O_4 incorporated epoxy coatings from Cure Index perspective. *Prog. Org. Coat.* **2019**, *133*, 220–228. [[CrossRef](#)]
20. Xie, H.; Liu, B.; Yuan, Z.; Shen, J.; Cheng, R. Cure kinetics of carbon nanotube/tetrafunctional epoxy nanocomposites by isothermal differential scanning calorimetry. *J. Polym. Sci. Part B Polym. Phys.* **2004**, *42*, 3701–3712. [[CrossRef](#)]
21. Sbirrazzuoli, N.; Vyazovkin, S.; Mititelu, A.; Sladic, C.; Vincent, L. A study of epoxy-amine cure kinetics by combining isoconversional analysis with temperature modulated DSC and dynamic rheometry. *Macromol. Chem. Phys.* **2003**, *204*, 1815–1821. [[CrossRef](#)]
22. Jouyandeh, M.; Ganjali, M.R.; Ali, J.A.; Aghazadeh, M.; Stadler, F.J.; Saeb, M.R. Curing epoxy with electrochemically synthesized $\text{Mn}_x\text{Fe}_3\text{-xO}_4$ magnetic nanoparticles. *Prog. Org. Coat.* **2019**, *136*, 105199. [[CrossRef](#)]
23. Jouyandeh, M.; Ganjali, M.R.; Ali, J.A.; Aghazadeh, M.; Stadler, F.J.; Saeb, M.R. Curing epoxy with electrochemically synthesized $\text{Co}_x\text{Fe}_3\text{-xO}_4$ magnetic nanoparticles. *Prog. Org. Coat.* **2019**, *137*, 105252. [[CrossRef](#)]
24. Jouyandeh, M.; Karami, Z.; Ali, J.A.; Karimzadeh, I.; Aghazadeh, M.; Laoutid, F.; Vahabi, H.; Saeb, M.R.; Ganjali, M.R.; Dubois, P. Curing epoxy with polyethylene glycol (PEG) surface-functionalized $\text{Ni}_x\text{Fe}_3\text{-xO}_4$ magnetic nanoparticles. *Prog. Org. Coat.* **2019**, *136*, 105250. [[CrossRef](#)]
25. Akbari, V.; Jouyandeh, M.; Paran, S.M.R.; Ganjali, M.R.; Abdollahi, H.; Vahabi, H.; Ahmadi, Z.; Formela, K.; Esmaeili, A.; Mohaddespour, A. Effect of Surface Treatment of Halloysite Nanotubes (HNTs) on the Kinetics of Epoxy Resin Cure with Amines. *Polymers* **2020**, *12*, 930. [[CrossRef](#)]
26. Tikhani, F.; Moghari, S.; Jouyandeh, M.; Laoutid, F.; Vahabi, H.; Saeb, M.R.; Dubois, P. Curing Kinetics and Thermal Stability of Epoxy Composites Containing Newly Obtained Nano-Scale Aluminum Hypophosphite (AlPO_2). *Polymers* **2020**, *12*, 644. [[CrossRef](#)]
27. Jouyandeh, M.; Ganjali, M.R.; Seidi, F.; Xiao, H.; Saeb, M.R. Nonisothermal Cure Kinetics of Epoxy/Polyvinylpyrrolidone Functionalized Superparamagnetic Nano- Fe_3O_4 Composites: Effect of Zn and Mn Doping. *J. Compos. Sci.* **2020**, *4*, 55. [[CrossRef](#)]

28. Saeb, M.R.; Nonahal, M.; Rastin, H.; Shabaniyan, M.; Ghaffari, M.; Bahlakeh, G.; Ghiyasi, S.; Khonakdar, H.A.; Goodarzi, V.; Puglia, D. Calorimetric analysis and molecular dynamics simulation of cure kinetics of epoxy/chitosan-modified Fe₃O₄ nanocomposites. *Prog. Org. Coat.* **2017**, *112*, 176–186. [[CrossRef](#)]
29. Jouyandeh, M.; Karami, Z.; Jazani, O.M.; Formela, K.; Paran, S.M.R.; Jannesari, A.; Saeb, M.R. Curing epoxy resin with anhydride in the presence of halloysite nanotubes: The contradictory effects of filler concentration. *Prog. Org. Coat.* **2019**, *126*, 129–135. [[CrossRef](#)]
30. Karami, Z.; Jouyandeh, M.; Hamad, S.M.; Ganjali, M.R.; Aghazadeh, M.; Torre, L.; Puglia, D.; Saeb, M.R. Curing epoxy with Mg-Al LDH nanoplatelets intercalated with carbonate ion. *Prog. Org. Coat.* **2019**, *136*, 105278. [[CrossRef](#)]
31. Karami, Z.; Jouyandeh, M.; Ali, J.A.; Ganjali, M.R.; Aghazadeh, M.; Maadani, M.; Rallini, M.; Luzi, F.; Torre, L.; Puglia, D.; et al. Development of Mg-Zn-Al-CO₃ ternary LDH and its curability in epoxy/amine system. *Prog. Org. Coat.* **2019**, *136*, 105264. [[CrossRef](#)]
32. Karami, Z.; Jouyandeh, M.; Ghiyasi, S.; Ali, J.A.; Ganjali, M.R.; Aghazadeh, M.; Maadani, M.; Rallini, M.; Luzi, F.; Torre, L.; et al. Exploring curing potential of epoxy nanocomposites containing nitrate anion intercalated Mg-Al-LDH with Cure Index. *Prog. Org. Coat.* **2020**, *139*, 105255. [[CrossRef](#)]
33. Vyazovkin, S.; Burnham, A.K.; Criado, J.M.; Pérez-Maqueda, L.A.; Popescu, C.; Sbirrazzuoli, N. ICTAC Kinetics Committee recommendations for performing kinetic computations on thermal analysis data. *Thermochim. Acta* **2011**, *520*, 1–19. [[CrossRef](#)]
34. Karami, Z.; Aghazadeh, M.; Jouyandeh, M.; Zarrintaj, P.; Vahabi, H.; Ganjali, M.R.; Torre, L.; Puglia, D.; Saeb, M.R. Epoxy/Zn-Al-CO₃ LDH nanocomposites: Curability assessment. *Prog. Org. Coat.* **2020**, *138*, 105355. [[CrossRef](#)]
35. Karami, Z.; Jazani, O.M.; Navarchian, A.H.; Saeb, M.R. State of cure in silicone/clay nanocomposite coatings: The puzzle and the solution. *Prog. Org. Coat.* **2018**, *125*, 222–233. [[CrossRef](#)]
36. Dimier, F.; Sbirrazzuoli, N.; Vergnes, B.; Vincent, M. Curing kinetics and chemorheological analysis of polyurethane formation. *Polym. Eng. Sci.* **2004**, *44*, 518–527. [[CrossRef](#)]
37. Wan, J.; Li, C.; Bu, Z.-Y.; Xu, C.-J.; Li, B.-G.; Fan, H. A comparative study of epoxy resin cured with a linear diamine and a branched polyamine. *Chem. Eng. J.* **2012**, *188*, 160–172. [[CrossRef](#)]
38. Domínguez, J.; Grivel, J.-C.; Madsen, B. Study on the non-isothermal curing kinetics of a polyfurfuryl alcohol bioresin by DSC using different amounts of catalyst. *Thermochim. Acta* **2012**, *529*, 29–35. [[CrossRef](#)]
39. Vyazovkin, S. Model-free kinetics. *J. Therm. Anal. Calorim.* **2006**, *83*, 45–51. [[CrossRef](#)]
40. Miura, K. A new and simple method to estimate f (E) and k₀ (E) in the distributed activation energy model from three sets of experimental data. *Energy Fuels* **1995**, *9*, 302–307. [[CrossRef](#)]
41. Saeb, M.R.; Rastin, H.; Shabaniyan, M.; Ghaffari, M.; Bahlakeh, G. Cure kinetics of epoxy/ β -cyclodextrin-functionalized Fe₃O₄ nanocomposites: Experimental analysis, mathematical modeling, and molecular dynamics simulation. *Prog. Org. Coat.* **2017**, *110*, 172–181. [[CrossRef](#)]
42. Seidi, F.; Jouyandeh, M.; Akbari, V.; Paran, S.M.R.; Livi, S.; Ducos, F.; Vahabi, H.; Ganjali, M.R.; Saeb, M.R. Super-crosslinked ionic liquid-intercalated montmorillonite/epoxy nanocomposites: Cure kinetics, viscoelastic behavior and thermal degradation mechanism. *Polym. Eng. Sci.* **2020**, *6*, e03798. [[CrossRef](#)]
43. Jouyandeh, M.; Tikhani, F.; Shabaniyan, M.; Movahedi, F.; Moghari, S.; Akbari, V.; Gabrion, X.; Laheurte, P.; Vahabi, H.; Saeb, M.R. Synthesis, characterization, and high potential of 3D metal-organic framework (MOF) nanoparticles for curing with epoxy. *J. Alloys Compd.* **2020**, *829*, 154547. [[CrossRef](#)]
44. Jouyandeh, M.; Zarrintaj, P.; Ganjali, M.R.; Ali, J.A.; Karimzadeh, I.; Aghazadeh, M.; Ghaffari, M.; Saeb, M.R. Curing epoxy with electrochemically synthesized GdxFe₃-xO₄ magnetic nanoparticles. *Prog. Org. Coat.* **2019**, *136*, 105245. [[CrossRef](#)]
45. Costa, D.G.; Rocha, A.B.; Souza, W.F.; Chiaro, S.S.X.; Leitão, A.A. Comparative Structural, thermodynamic and electronic analyses of ZnAlAn- hydrotalcite-like compounds (An⁻ Cl⁻, F⁻, Br⁻, OH⁻, CO₃²⁻ or NO₃⁻): An ab initio study. *Appl. Clay Sci.* **2012**, *56*, 16–22. [[CrossRef](#)]
46. Jouyandeh, M.; Paran, S.M.R.; Khadem, S.S.M.; Ganjali, M.R.; Akbari, V.; Vahabi, H.; Saeb, M.R. Nonisothermal cure kinetics of epoxy/MnxFe₃-xO₄ nanocomposites. *Prog. Org. Coat.* **2020**, *140*, 105505. [[CrossRef](#)]
47. Jouyandeh, M.; Yarahmadi, E.; Didehban, K.; Ghiyasi, S.; Paran, S.M.R.; Puglia, D.; Ali, J.A.; Jannesari, A.; Saeb, M.R.; Ranjbar, Z.; et al. Cure kinetics of epoxy/graphene oxide (GO) nanocomposites: Effect of starch functionalization of GO nanosheets. *Prog. Org. Coat.* **2019**, *136*, 105217. [[CrossRef](#)]

48. Málek, J. A computer program for kinetic analysis of non-isothermal thermoanalytical data. *Thermochim. Acta* **1989**, *138*, 337–346. [[CrossRef](#)]
49. Montserrat, S.; Málek, J. A kinetic analysis of the curing reaction of an epoxy resin. *Thermochim. Acta* **1993**, *228*, 47–60. [[CrossRef](#)]
50. Peng, W.; Liu, Y.; Lu, Z.; Hu, J.; Zeng, K.; Yang, G. Curing kinetics study on highly efficient thermal synergistic polymerization effect between alicyclic imide moiety and phthalonitrile. *Thermochim. Acta* **2018**, *659*, 27–33. [[CrossRef](#)]
51. Jouyandeh, M.; Karami, Z.; Hamad, S.M.; Ganjali, M.R.; Akbari, V.; Vahabi, H.; Kim, S.-J.; Zarrintaj, P.; Saeb, M.R. Nonisothermal cure kinetics of epoxy/Zn_xFe_{3-x}O₄ nanocomposites. *Prog. Org. Coat.* **2019**, *136*, 105290. [[CrossRef](#)]
52. Bello, R.H.; Coelho, L.A. Curing kinetics of chemically recyclable thermoset and their nanocomposites. *Thermochim. Acta* **2019**, *679*, 178317. [[CrossRef](#)]
53. Karami, Z.; Ganjali, M.R.; Zarghami Dehaghani, M.; Aghazadeh, M.; Jouyandeh, M.; Esmaili, A.; Habibzadeh, S.; Mohaddespour, A.; Formela, K.; Haponiuk, J.T. Kinetics of Cross-Linking Reaction of Epoxy Resin with Hydroxyapatite-Functionalized Layered Double Hydroxides. *Polymers* **2020**, *12*, 1157. [[CrossRef](#)] [[PubMed](#)]
54. Jouyandeh, M.; Ganjali, M.R.; Ali, J.A.; Aghazadeh, M.; Paran, S.M.R.; Naderi, G.; Saeb, M.R.; Thomas, S. Curing epoxy with polyvinylpyrrolidone (PVP) surface-functionalized Zn_xFe_{3-x}O₄ magnetic nanoparticles. *Prog. Org. Coat.* **2019**, *136*, 105227. [[CrossRef](#)]
55. Wang, Z.; Liu, L.; Zhang, J.; Cao, L.; Dong, H.; Zhang, C.; Xu, X.; Zhu, M.; Li, J. Optimizing curing process of graphene oxide/waterborne epoxy blends by curing kinetics simulation considering the coupling of heat conduction and curing reaction. *Thermochim. Acta* **2019**, *672*, 60–69. [[CrossRef](#)]
56. Kissinger, H.E. Reaction kinetics in differential thermal analysis. *Anal. Chem.* **1957**, *29*, 1702–1706. [[CrossRef](#)]
57. Akahira, T.; Sunose, T. Res. Report Chiba Inst. *Technol. Sci. Technol* **1971**, *16*, 22.
58. Sbirrazzuoli, N. Is the Friedman method applicable to transformations with temperature dependent reaction heat? *Macromol. Chem. Phys.* **2007**, *208*, 1592–1597. [[CrossRef](#)]
59. Ozawa, T. Kinetic analysis of derivative curves in thermal analysis. *J. Therm. Anal. Calorim.* **1970**, *2*, 301–324. [[CrossRef](#)]
60. Tao, Q.; Su, L.; Frost, R.L.; He, H.; Theng, B.K.G. Effect of functionalized kaolinite on the curing kinetics of cycloaliphatic epoxy/anhydride system. *Appl. Clay Sci.* **2014**, *95*, 317–322. [[CrossRef](#)]
61. Zhou, T.; Gu, M.; Jin, Y.; Wang, J. Studying on the curing kinetics of a DGEBA/EMI-2, 4/nano-sized carborundum system with two curing kinetic methods. *Polymer* **2005**, *46*, 6174–6181. [[CrossRef](#)]
62. Li, L.; Zeng, Z.; Zou, H.; Liang, M. Curing characteristics of an epoxy resin in the presence of functional graphite oxide with amine-rich surface. *Thermochim. Acta* **2015**, *614*, 76–84. [[CrossRef](#)]

